Development of State-of-the-Art Proof-Test Methodology

Charles L. Denniston/ED25
205–544–7248

MSFC is currently funding the Southwest Research Institute to provide the Center with an updated, state-of-the-art, proof-testing guidelines document for metallic pressure vessels. The current guidelines document, NASA–SP–8040, was released in 1970, is out of date, and is based on a linear analysis approach that is no longer in wide use.

Southwest Research is utilizing two new pieces of technology to develop the new document. The first piece provides a way of solving elastic-plastic fracture mechanics problems by estimating a flaw's *J*-integral value via the Electric Power Research Institute *J*-integral estimation scheme. The second technology being incorporated into the evolving guidelines document is the Failure Assessment Diagram, which is to be used to evaluate flaw growth behavior, including the initiation of ductile tearing and instability in the vicinity of the flow. Both of the approaches represent relatively new ways to solve the type of fracture mechanics problems faced when an engineer designs proof tests.

The *J*-integral estimation scheme provides a means for estimating the *J*-integral value for a flaw responding to a particular loading in a certain geometry. While methods for calculating actual *J*-integral values for flaws do exist, these solutions are only for a limited range of problem types and are not generally easy to determine. The Electric Power Research Institute scheme approaches the problem of estimating *J*-integrals by assuming the total *J*-integral for a particular problem can be expressed as the sum of exclusively elastic and purely plastic solutions.

$$J_{\text{Total}} = J_e + J_p$$

The J_e term represents the elastic portion of the total *J*-integral and is defined as:

$$J_e = \frac{K^2(a_e)}{E'} \text{ with :}$$

$$E' = \begin{cases} E; & \text{for plane stress} \\ \dfrac{E}{(1-\mu^2)}; & \text{for plane strain} \end{cases}$$

where:
$K(a_e)$ = Linear stress intensity factor (pounds per square inch $\sqrt{\text{inch}}$)
a_e = An equivalent crack size (inches)
E = Material's modulus of elasticity (pounds per square inch)
m = Material's Poisson's ratio $\left(\text{inch}/\text{inch}\right)$.

The nonlinear (plastic) contribution to the total *J*-integral is:

$$J_p = \alpha(\sigma_0)(\varepsilon_0)(\mathrm{c})(h_1\{a, n\})\left(\frac{P}{P_0}\right)^{n+1}$$

where:
a = Ramberg-Osgood equation constant
s_0 = Material's yield strength (pounds per square inch)
e_0 = Corresponding strain to s_0
c = Uncracked ligament length (inches)
h_1 = Electric Power Research Institute elastic-plastic fracture mechanics expression (function of material and geometry)
a = Actual crack size [or depth] (inches)
n = Ramberg-Osgood equation exponent
P = Applied load [either tensile (pound mass force) or moment (inches per pound mass force)]
P_0 = Characterizing yield load (pound mass force or inches per pound mass force).

The estimation of the *J*-integral for a particular problem now only involves the acquisition of what is generally readily available information.

Obtaining a value for a flaws *J*-integral is a vital part of any proof-test philosophy, but it is not sufficient. As an example, one only has to consider a leak-before-burst calculation for a potential flaw in the side of a thin-walled pressure vessel consisting of a ductile metal. This type of leak-before-burst problem can easily become a nonlinear problem with significant yielding around the flaw when pressures are high. The yielding complicates the calculation of a *J*-integral and reduces the material's resistance to failure. Any proof-test philosophy that will work with thin-walled pressure vessels of ductile metals must be capable of handling this loss of toughness brought about with increased local loading.

Southwest Research plans to account for this loss of toughness in the guidelines they are developing by using Failure Assessment Diagrams. Figure 81 provides an example in which the "failure curve" illustrates the reduction in material toughness with increased loading. The K_r and L_r terms are defined below.

$$K_r = f\left\{\frac{\sqrt{J_{\text{Apply}}}}{\sqrt{J_{\text{Apply}}}}\right\};$$

$$L_r = g\left\{\frac{P_{\text{Applied}}}{P_{\text{Reference}}}\right\}$$

Failure Assessment Diagrams can be used to do more than just determine material allowables. They can also be used to solve flaw-tearing problems in ductile metals. Figure 81 illustrates a situation where a certain flaw is growing due to a constant load, P. When the flaw growth reaches point B, initiation of tearing is predicted. At the flaw's tip, the stress and *J*-integral can be predicted by using the corresponding K_r and L_r values at point B. Tearing is predicted to be arrested at point C, where the stress and *J*-integral at tearing arrest can be determined from examining the K_r and L_r values corresponding to that point. However, if the "increasing tear" curve were tangent to the "failure curve," then the instability of the flaw would be imminent, and the tearing of the flaw might not stop. In such a case, a failure, e.g., a pipe burst, would be predicted.

Southwest Research is currently running tests to verify the Failure Assessment Diagram approach to predicting tearing behavior. In figure 82, a plot comparing the measured critical crack depth to the predicted critical crack depth is shown for surface flaws in Inconel 718 test specimens. A similar plot could be shown for measured versus predicted critical loads. Southwest has been able to predict the initiation and instability behavior of tearing flaws generally within ±10 percent.

The final phase of testing to verify the philosophy to be incorporated into the proof-testing guidelines is underway. In the final phase of Failure Assessment Diagram testing, space shuttle main engine ducts are having surface flaws placed in them and their ends sealed. Each of these three ducts will then be pressurized until failure. The growth of each flaw placed in the duct wall will be examined and compared to what the approach to be incorporated into the proof-testing guidelines predicts. Once these three tests are completed, the actual writing of guidelines should commence. The proof-testing guidelines document is scheduled to be delivered to MSFC by the end of the 1996 fiscal year.

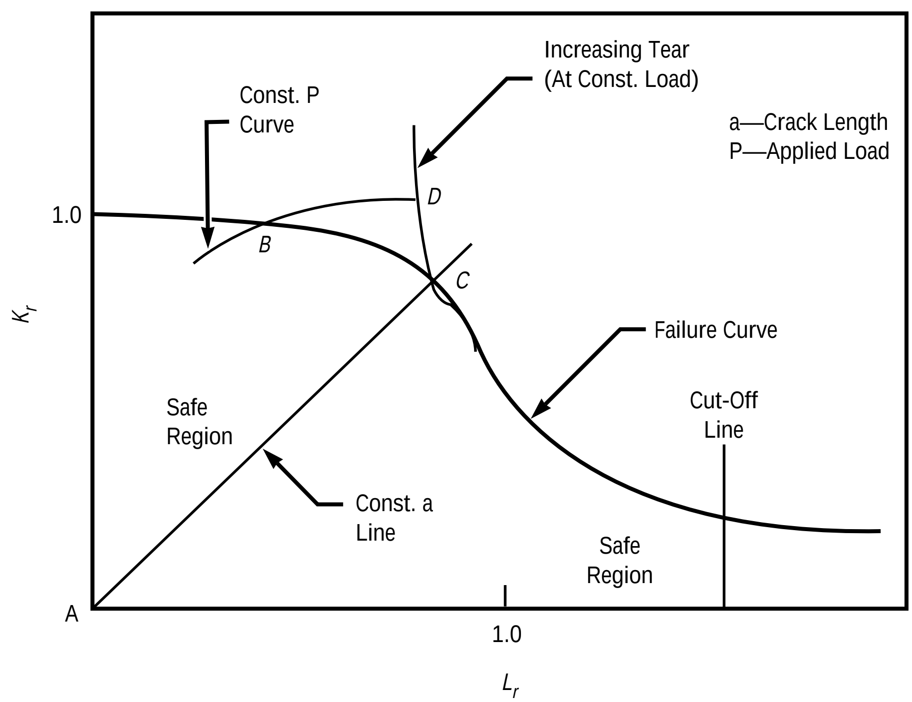

Figure 81.—Failure Assessment Diagram with tearing.

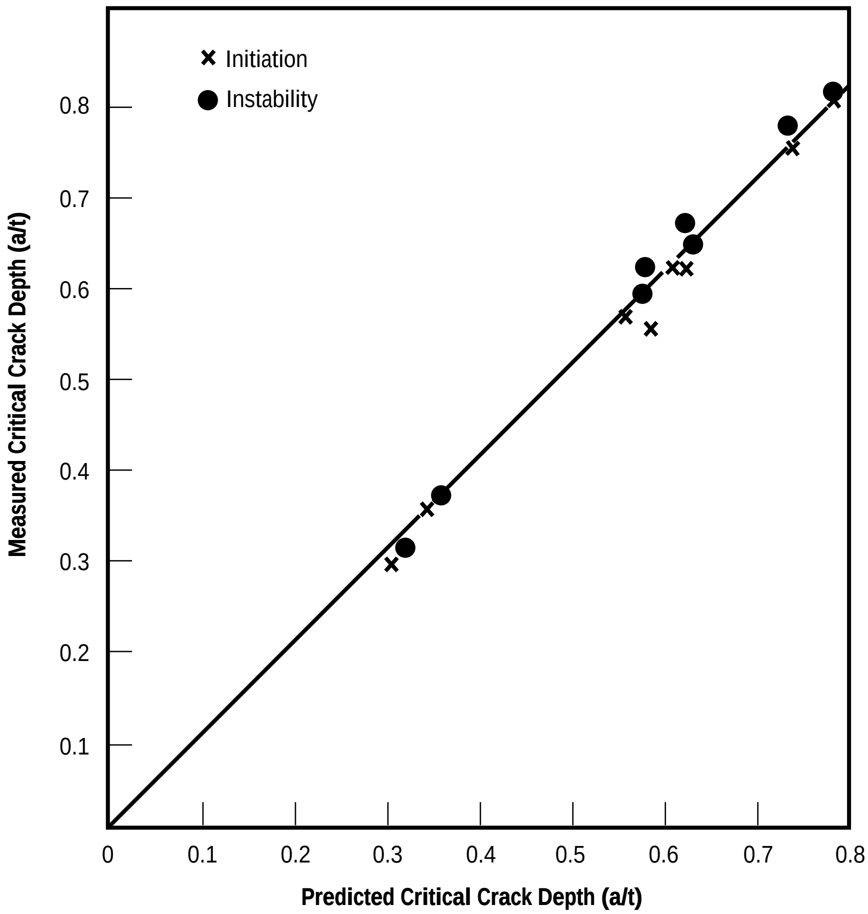

Figure 82.—Comparison of measured and predicted crack depths at the initiation of stable tearing and instability for Inconel 718 test specimens.

Sponsor: Office of Space Access and Technology

Industry Involvement: Southwest Research Institute